







Many-particle effects in optical transitions from zero-mode Landau levels in HgTe quantum wellsS. S. Krishtopenko ¹, A. M. Kadykov ¹, S. Gebert ², S. Ruffenach,¹ C. Consejo,¹ J. Torres ², C. Avogadri,¹ B. Jouault ¹, W. Knap,¹ N. N. Mikhailov,^{3,4} S. A. Dvoretiskii,^{3,4} and F. Teppe ^{1,*}¹Laboratoire Charles Coulomb, Université de Montpellier, Centre National de la Recherche Scientifique, 34095 Montpellier, France²Institut d'Electronique et des Systèmes, Université de Montpellier, Centre National de la Recherche Scientifique, 34000 Montpellier, France³Institute of Semiconductor Physics, Siberian Branch, Russian Academy of Sciences,
pr. Akademika Lavrent'eva 13, Novosibirsk, 630090 Russia⁴Novosibirsk State University, Pirogova st. 2, 630090 Novosibirsk, Russia

(Received 10 December 2019; revised 27 April 2020; accepted 13 July 2020; published 31 July 2020)

We report on the far-infrared magnetospectroscopy of HgTe quantum wells with inverted band ordering at different electron concentrations. We particularly focus on optical transitions from zero-mode Landau levels, which split from the edges of electronlike and holelike bands. We observe a pronounced dependence of the transition energies on the electron concentration varied by persistent photoconductivity effect. This is striking evidence that in addition to the already well-documented crystalline and interface asymmetries, electron-electron interactions also have a significant impact on the usual behavior of the optical transitions from zero-mode Landau levels.

DOI: [10.1103/PhysRevB.102.041404](https://doi.org/10.1103/PhysRevB.102.041404)

HgTe/CdTe quantum wells (QWs) were the first known two-dimensional (2D) systems, in which the band ordering depended strongly on the QW width d [1]. If d is smaller than a critical value d_c , the first electronlike ($E1$) subband in the QW lies above the first holelike ($H1$) subband, and the QW has a trivial band ordering [2]. In wide QWs, when $d > d_c$, $E1$ falls below $H1$ and the band ordering becomes inverted, giving rise to the 2D topological insulator state [2,3]. At critical QW width, $d = d_c$, HgTe QWs host a gapless state with massless Dirac fermions [4–7]. The band ordering in HgTe QWs can also be changed by hydrostatic pressure [8], temperature [9,10], strain [11,12], or disorder [13].

The most efficient way to discriminate trivial and inverted band ordering in HgTe QWs is to probe the evolution of a particular pair of Landau levels (LLs) under applied magnetic field [3]. These so-called *zero-mode* LLs split from the edges of $E1$ and $H1$ subbands and have pure electronlike and holelike character, respectively. The energy of the electronlike zero-mode LL increases with magnetic field, while the energy of that of the $H1$ subband decreases as the field increases. In inverted HgTe QWs, the zero-mode LLs therefore cross at a critical magnetic field B_c (Fig. 1), above which the inverted band ordering transforms into the trivial one [3].

The presence of bulk inversion asymmetry (BIA) [14,15] in the unit cell of zinc-blende materials, as well as the interface inversion asymmetry (IIA) at the HgTe/CdHgTe heterojunction [16] induce the anticrossing of zero-mode LLs in the vicinity of B_c . It appears that the value of this anticrossing gap Δ depends considerably on the experimental technique used to measure it. Particularly, the measurements of magnetotransport [4,5,17,18] and photoconductivity [19,20] performed with gated Hall bars show that the anticrossing

gap is negligibly small. On the contrary, the far-infrared magnetospectroscopy reveals a fine structure of the optical transitions from zero-mode LLs [21–24]. The analysis of this fine structure in the vicinity of B_c within the Dirac-like model, including BIA and IIA, gives $\Delta \sim 5$ meV for the joint effects. These contested experimental values of the anticrossing gap obtained in magnetotransport and magnetospectroscopy triggered a vivid discussion about the real strength of BIA and IIA in HgTe QWs [5,24–26].

The key difference between magnetotransport and far-infrared magnetospectroscopy is that the latter induces inter-LL excitations, which may be considered as neutral collective modes [27,28] or *magnetic excitons* [28] composed of a bound state of a hole in a filled LL and an electron in an otherwise empty level. The long-wavelength limit of certain magnetic excitons [27,28], such as magnetoplasmons, contributes into magneto-optical conductivity, defining the resonant energy and intensity of the magnetoabsorption lines [29,30].

In 2D systems with parabolic band dispersion, all inter-LL transitions contributing into magnetoabsorption have the same cyclotron resonance (CR) energy, which is known to be insensitive to electron-electron ($e-e$) interaction [29,31]. Nonparabolic 2D systems have multiple LL transitions with different energies corresponding to multiple magnetoplasmonic modes [29,30]. In such systems, the $e-e$ interaction mixes collective modes having close energies, already at zero wave vector, making magneto-optical conductivity sensitive to many-particle effects [32,33]. So far, many-particle effects in magnetospectroscopy were observed in InAs QWs [32–37] and graphene [38–41]. As HgTe QWs also have strongly nonparabolic band structure [2,3], many-particle effects should also contribute to their magneto-optical conductivity.

Here, we study the evolution of optical transitions from the zero-mode LLs in inverted HgTe QWs at different electron concentrations varied by the persistent photoconductivity

*frederic.teppe@umontpellier.fr

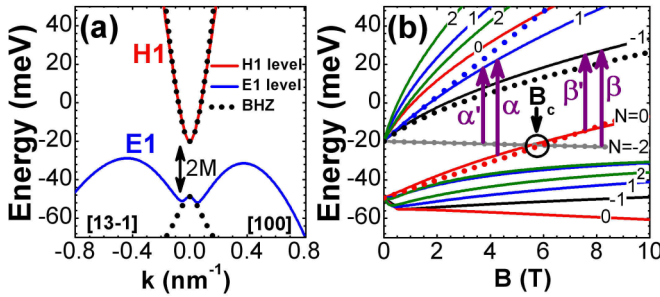


FIG. 1. Band structure (a) and Landau levels (b) of rectangular 8-nm-wide HgTe/Cd_{0.7}Hg_{0.3}Te QWs at $T = 2$ K. (a) The blue and red curves represent band dispersion of $E1$ and $H1$ subbands, calculated within the eight-band $\mathbf{k}\cdot\mathbf{p}$ Hamiltonian [8]. The dotted curves show the dispersion within the BHZ model [2]. (b) The numbers over the curves show the LL indices within the eight-band $\mathbf{k}\cdot\mathbf{p}$ Hamiltonian [8]. The arrows represent LL transitions observed in the vicinity of B_c [7,21–23]. The dotted colored curves show the corresponding LLs calculated within the BHZ model by using parameters provided in the Supplemental Material [44].

effect [42,43]. By fitting the difference in the transition energies with an analytical expression including BIA and IIA, we extract the energy gap at the Γ point of the Brillouin zone, the anticrossing gap Δ , and the critical magnetic field B_c from our experimental data. An unexpected strong dependence of the energy gap on the electron concentration clearly evidences that e - e interaction affects the LL transitions beyond the single-particle picture.

Let us first consider the typical band structure and LLs of inverted HgTe QWs in the absence of BIA and IIA (see Fig. 1). The calculations were performed using the eight-band $\mathbf{k}\cdot\mathbf{p}$ Hamiltonian [8]. We also neglect the structure inversion asymmetry (SIA) assuming that the QW profile is symmetrical. To calculate the LLs, we apply the axial approximation by omitting the warping terms in the Hamiltonian [8]. In this case, the electron-wave function for a given LL index $N > 0$ generally has eight components, describing the contribution of the Γ_6 , Γ_7 , and Γ_8 bands into the LL. We note that a specific LL with $N = -2$ contains only a contribution of the heavy-hole band with a momentum projection $\pm 3/2$ [8,21,22]. Details of the LL notation within the eight-band $\mathbf{k}\cdot\mathbf{p}$ Hamiltonian are provided in Ref. [8].

The absence of BIA and IIA implies that the two zero-mode LLs, which can be recognized in the LLs with $N = -2$ and $N = 0$ in Fig. 1, simply cross each other at a critical magnetic field B_c [8,21,22]. In this case, optically active inter-LL transitions follow conventional $\Delta N = \pm 1$ selection rules imposed by angular momentum conservation law [21]. Transitions from the zero-mode LLs, which follow these selection rules are marked in Fig. 1 as α and β transitions, in accordance with the notation of Schultz *et al.* [45]. On the contrary, the α' and β' transitions from the zero-mode LLs both correspond to “spin-flip” transitions [3,6], which are forbidden in the single-particle picture if BIA and IIA are ignored.

The inter-LL transitions can be also analytically described within the Dirac-like model proposed by Bernevig, Hughes, and Zhang (BHZ) [2,3]. This BHZ model is directly derived

from the eight-band $\mathbf{k}\cdot\mathbf{p}$ Hamiltonian by applying a perturbation approach for the QW states in the vicinity of the Γ point [2]. By using parameters provided in the Supplemental Material [44], one can see that the BHZ model well describes the electronic states at small values of \mathbf{k} [see Fig. 1(a)]. The colored dotted curves in Fig. 1(b) show the energy of LLs involved in α , α' , β , and β' transitions calculated within the BHZ model.

It is seen that only the energies of the zero-mode LLs are in good agreement with realistic numerical calculations. The difference in the energies calculated within both models does not exceed 10% for the zero-mode LL from the $E1$ subband, while the final levels of α , α' , β , and β' transitions show a significant deviation. However, by combining the energies of α with α' transition and β with β' transition, we exclude the “wrong” LLs from consideration and apply the BHZ model to the energy difference:

$$\Delta E = \frac{\hbar\omega_{\alpha'} - \hbar\omega_{\alpha}}{2} = \frac{\hbar\omega_{\beta'} - \hbar\omega_{\beta}}{2} = \frac{\epsilon_0^{(+)} - \epsilon_0^{(-)}}{2}, \quad (1)$$

where $\epsilon_0^{(+)}$ and $\epsilon_0^{(-)}$ are the energies of the zero-mode LLs from the $E1$ and $H1$ subband, respectively. In the presence of SIA, BIA, and IIA, the energies $\epsilon_0^{(\pm)}$ can be calculated analytically within the BHZ model [44]:

$$\Delta E = \sqrt{M^2 \left(1 - \frac{B}{B_c}\right)^2 + \frac{\Delta^2}{4}}, \quad (2)$$

where Δ is the anticrossing gap at $B = B_c$ caused by both BIA and IIA, while B_c and M are the critical field and the mass parameter, respectively, both introduced in the absence of BIA and IIA [44]. The parameter M defines the gap between the $E1$ and $H1$ subbands at the Γ point of the Brillouin zone (see Fig. 1): it is positive for trivial band ordering and negative for inverted band structure. Thus, by fitting experimental values of the energy differences for both pairs of the transitions, one can directly extract the values of Δ , B_c , and M from magnetoabsorption. We note that, in contrast to the band structure shown in Fig. 1, Eq. (2) is also valid for asymmetrical QWs [44].

In this work, we have studied three different samples, each containing an 8-nm-wide HgTe QW embedded between Cd_xHg_{1-x}Te barriers: $x = 0.62$ for sample 091223, $x = 0.41$ for sample 101221 and $x = 0.77$ for sample 101109. The samples were grown by molecular beam epitaxy on a semi-insulating (013) GaAs substrate with a relaxed CdTe buffer [46]. The barriers were selectively doped with indium, resulting in a 2D electron concentration n_s of a few 10^{11} cm⁻² at low temperatures. The magnetoabsorption spectra were measured in the Faraday configuration at 2 K by using a Fourier transform spectrometer coupled to a 16-T superconducting coil [47]. All spectra were normalized by the sample transmission at zero magnetic field. In the measurements, the electron concentration was varied through the persistent photoconductivity effect [42,43] by changing the time of illumination with a blue light emitting diode (LED). We note that illumination of HgTe QWs with blue LED results in increasing of n_s [48], in contrast to the case of InAs/GaSb QWs [43]. The concentration values were determined via magnetotransport measurements in the van der Pauw geometry.

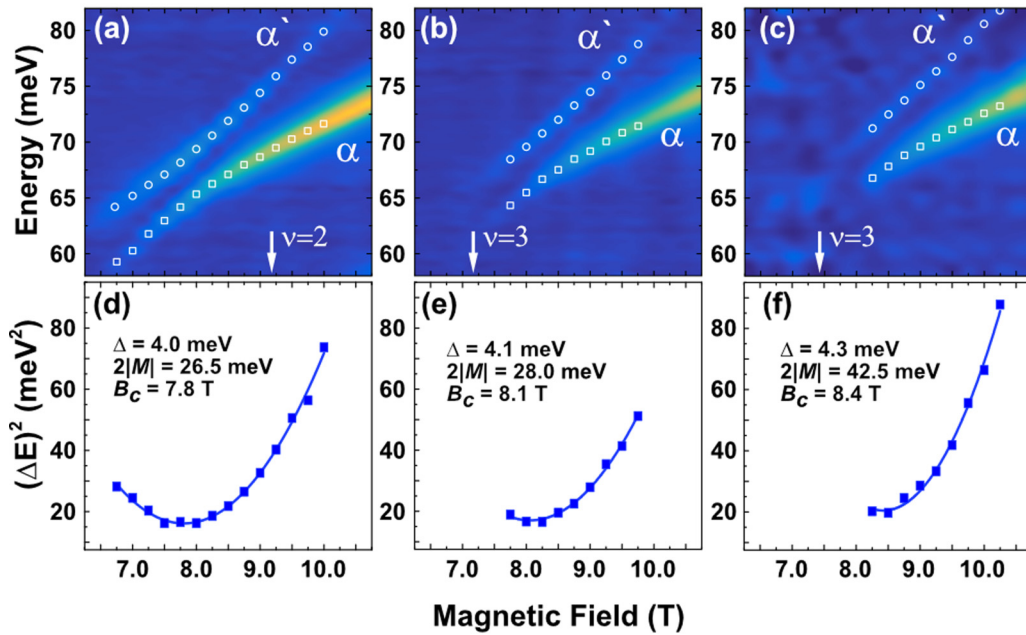


FIG. 2. (a)–(c) Color maps showing α and α' inter-LL transitions in the 8-nm HgTe/Cd_{0.77}Hg_{0.27}Te QW (sample 101109) as a function of magnetic field, measured at different electron concentration n_S : (a) 4.5×10^{11} cm⁻², (b) 5.3×10^{11} cm⁻², (c) 5.7×10^{11} cm⁻². The symbols represent the position of the magnetoabsorption lines, whose energies are used in the evaluation of ΔE . (d)–(f) Square of the energy difference for α and α' transitions at the same concentrations as in the respective top panels. The solid curves are the fitting to Eq. (2). The arrows indicate magnetic fields corresponding to the integer filling factor ν .

The magnetoabsorption spectra for the samples 101109 and 091223 are shown in Figs. 2 and 3, respectively. The spectra of the sample 101221 are provided in the Supplemental

Material [44]. As we are interested in the fine structure of the α and β transitions in the vicinity of B_c , we only supply the high-energy parts of the spectra, above the reststrahlen

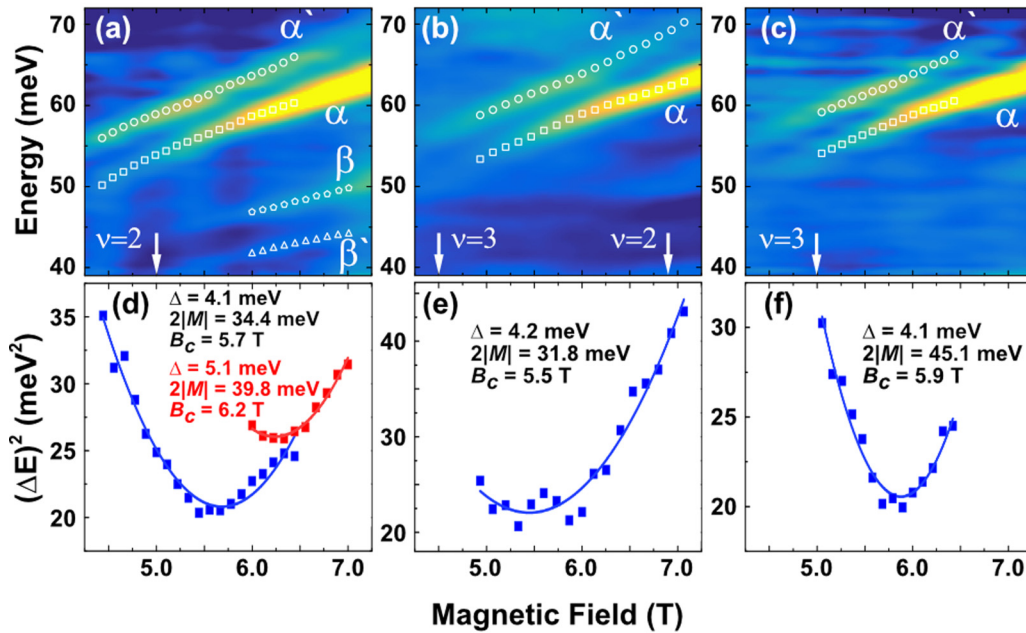


FIG. 3. (a)–(c) Color maps of the α , α' , β , and β' inter-LL transitions as a function of magnetic field in the 8-nm HgTe/Cd_{0.62}Hg_{0.38}Te QW (sample 091223) at different electron concentration n_S : (a) 2.4×10^{11} cm⁻², (b) 3.3×10^{11} cm⁻², (c) 3.6×10^{11} cm⁻². The symbols correspond to the position of the magnetoabsorption lines, whose energies are used in the evaluation of ΔE . (d)–(f) Square of the energy differences for both pairs of the transitions at the same concentrations as in the respective top panels. The solid curves are the fitting to Eq. (2). The red and blue colors correspond to the α - α' and β - β' anticrossing, respectively. The arrows indicate magnetic fields corresponding to the integer filling factor ν .

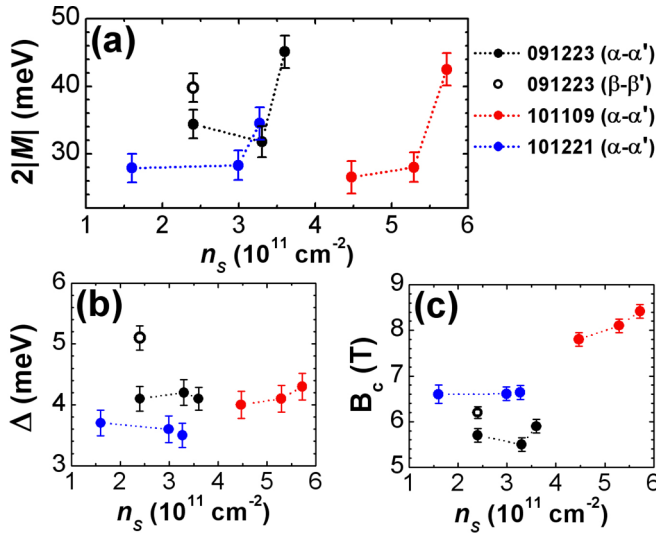


FIG. 4. Evolution of single-particle parameters with electron concentration extracted from magnetoabsorption of different samples: (a) $2|M|$ vs n_s , (b) B_c vs n_s , (c) Δ vs n_s .

band of the GaAs substrate (typically in the 30–40 meV range) [21,22]. The low-energy parts feature several CR-like transitions from higher LLs in the conduction band and look qualitatively the same, as in previous works [7,21–23].

The most intense line for the sample 101109 (see Fig. 2) is identified as the α transition accompanied by the weaker line of the α' transition. As seen from Fig. 1, the α and α' transitions are both present in the spectra if the filling factor of LLs ν in the conduction band is less than three. Indeed, $\nu < 3$ for the n_s values of $4.5 \times 10^{11} \text{ cm}^{-2}$, $5.3 \times 10^{11} \text{ cm}^{-2}$, $5.7 \times 10^{11} \text{ cm}^{-2}$ is fulfilled for magnetic fields higher than 6.2, 7.3, and 7.9 T, respectively. The absence of the β and β' transitions in the spectra of the sample 101109 is attributed to $\nu > 2$ in the given magnetic field range.

As seen from Fig. 3(a), $n_s = 2.4 \times 10^{11} \text{ cm}^{-2}$ allows for observation of all four α , α' , β , and β' transitions in the sample 091223 since $\nu < 2$ represents the fields higher than 5.0 T. Increasing of n_s up to $3.3 \times 10^{11} \text{ cm}^{-2}$ yields to the vanishing of the β and β' transitions in the field range of $4.5 \text{ T} < B < 6.8 \text{ T}$ since it corresponds to $2 < \nu < 3$. We note that the α' and β' transitions are observed just in the vicinity of B_c , while above the field range shown in Fig. 3, only the α and β transitions are present.

In order to analyze our magnetoabsorption data within the single-particle picture, we have fitted the difference in energies ΔE between α and α' , and between β and β' transitions by Eq. (2). As seen from Figs. 2 and 3, the energy difference is formally well described by the BHZ model including the SIA, BIA, and IIA effects. Figure 4 summarizes the values of Δ , B_c , and M as a function of n_s for both pairs of the transitions. The error bar for the extracted values does not exceed 10%.

In the following, we address some interesting features, which cannot be explained within the single-particle picture. First, the values of Δ , B_c , and M extracted from $\hbar\omega_{\alpha'} - \hbar\omega_{\alpha}$ and $\hbar\omega_{\beta'} - \hbar\omega_{\beta}$ differ significantly from each other. The difference between $\hbar\omega_{\alpha'} - \hbar\omega_{\alpha}$ and $\hbar\omega_{\beta'} - \hbar\omega_{\beta}$ is clearly seen in Fig. 3(d). Note that in the single-particle picture, the energy

differences $\hbar\omega_{\alpha'} - \hbar\omega_{\alpha}$ and $\hbar\omega_{\beta'} - \hbar\omega_{\beta}$ should be the same. This is a general property of the single-particle approach, which is still valid in the BHZ model [23].

Second, Fig. 4(a) demonstrates a pronounced dependence of the energy gap $2M$ on the electron concentration. The changing range for $2M$ exceeds significantly the error bar and the deviation within 10%, expected for zero-mode LLs in the BHZ model (see Fig. 1). On the other hand, Δ and B_c are either independent of n_s or have a weak concentration dependence within the error bar. Although the changing of n_s affects the band structure via the changes of the QW profile, such effect is small in our samples. Particularly, the self-consistent calculations involving the Poisson equation and the eight-band $\mathbf{k} \cdot \mathbf{p}$ Hamiltonian predict less than 5% changing of $2M$ for pure asymmetrical QWs in the range of n_s shown in Fig. 4. Thus, the strong concentration dependence of $2|M|$ together with the different values of Δ and B_c extracted from $\hbar\omega_{\alpha'} - \hbar\omega_{\alpha}$ and $\hbar\omega_{\beta'} - \hbar\omega_{\beta}$ cannot be interpreted within the single-particle picture.

Let us now discuss a qualitatively possible mechanism beyond the single-particle picture, which may result in the fine structure of α and β transitions shown in Figs. 2 and 3. As mentioned before, any inter-LL transition observed in magnetoabsorption can be considered as a neutral magnetic exciton, which long-wavelength limit contributes to the magneto-optical conductivity [27–30]. In this sense, two LL transitions with close energies, such as α and α' , correspond to two magnetic excitons with zero wave vectors. In the absence of e - e interaction, their energies are defined by the single-particle LLs and only the α exciton contributes in magnetoabsorption.

The many-particle interaction [27–30] gives rise to (1) an electron-hole interaction inside a given exciton (its bound energy); (2) interaction between excited exciton and other nonexcited electrons below the Fermi level; and (3) the exciton-exciton interaction caused by the interaction between the electrons and holes of the α and α' excitons. The first two interactions just change the energies of the α and α' excitons from its single-particle values. On the contrary, the interaction (3) induces hybridization between two magnetic excitons, which leads to nonzero α' contribution into magnetoabsorption and anticrossing between α and α' magneto-optical transitions.

This hybridization between the excitons is very efficient if the energies of α and α' transitions differ in less than the characteristic length of Coulomb interaction E_c in our samples. The latter can be roughly evaluated as $E_c \sim e^2/(a_B\epsilon)$, where e is an elementary charge, a_B is the magnetic length given by $a_B^2 = \hbar c/eH$, and $\epsilon = 21$ is the static permittivity of HgTe. In the field range of $B = 4$ –9 T, E_c changes from 5 to 8 meV, which is comparable with the experimental values of $\hbar\omega_{\alpha'} - \hbar\omega_{\alpha}$ and $\hbar\omega_{\beta'} - \hbar\omega_{\beta}$ in the vicinity of B_c . Therefore, it is relevant to account many-particle effects in the consideration of the fine structure of α and β transitions. Thus, the strong dependence of the band-gap energy in Fig. 4 is due to the inapplicability in the vicinity of B_c of the single-particle model described by Eq. (2).

Moreover, since the many-particle hybridization is sensitive to the electron concentration n_s and LL filling factor ν , it may indeed result in different fine structures for the

α and β transitions. Additionally, the proposed mechanism does not require the anticrossing of zero-mode LLs, which is consistent with experimental evidences of the small values of BIA and IIA obtained by magnetotransport [4,5,17,18] and photoconductivity [19,20].

Finally, we note that the previous magnetospectroscopy studies of HgTe QWs [6,7,21,22] have shown a good agreement between experimental values and single-electron calculations for all observed transitions in *trivial* QWs [6,7,22] and in *inverted* QWs in the field range far from B_c [7,21,22]. In these cases, the difference between the transition energies is greater than $E_c \sim e^2/(a_B\epsilon)$. The latter means that unlike in graphene, in which the LL transitions are affected by many-particle interaction in the whole range of magnetic fields [38–41], unhybridized optical transitions in HgTe QWs can be treated far from the critical field B_c within the single-electron picture.

In conclusion, we have studied inverted HgTe/CdHgTe QWs by far-infrared magnetospectroscopy, by varying the carrier density with a persistent photoconductivity effect. The

single-electron analysis of several optical transitions from the zero-mode LLs near their crossing, highlights the contribution of many-particle phenomena, via an unexpectedly strong dependence of the band-gap energy as a function of the electron concentration. This indicates that LL transitions from zero-mode LLs probed by far-infrared magnetospectroscopy should be considered in terms of magnetic excitons, as collective modes [27–30,32–34], hybridized by many-particle interaction.

The authors gratefully thank M. Orlita for the helpful discussions and critical comments. This work was supported by the MIPS Department of Montpellier University through the “Occitanie Terahertz Platform,” by CNRS through IRP “TeraMIR,” by the French Agence Nationale pour la Recherche (Colector project), and by the European Union through the Flag-Era JTC 2019–DeMeGras project and the ITN TeraApps - Marie Skłodowska-Curie Action (No. 765426) from Horizon 2020 Research and Innovation Programme.

-
- [1] L. G. Gerchikov and A. V. Subashiev, *Phys. Status Solidi B* **160**, 443 (1990).
- [2] B. A. Bernevig, T. L. Hughes, and S.-C. Zhang, *Science* **314**, 1757 (2006).
- [3] M. König, S. Wiedmann, C. Brüne, A. Roth, H. Buhmann, L. W. Molenkamp, X.-L. Qi, and S.-C. Zhang, *Science* **318**, 766 (2007).
- [4] B. Büttner, C. Liu, G. Tkachov, E. Novik, C. Brüne, H. Buhmann, E. Hankiewicz, P. Recher, B. Trauzettel, S. Zhang, and L. Molenkamp, *Nat. Phys.* **7**, 418 (2011).
- [5] A. M. Kadykov, S. S. Krishtopenko, B. Jouault, W. Desrat, W. Knap, S. Ruffenach, C. Consejo, J. Torres, S. V. Morozov, N. N. Mikhailov, S. A. Dvoretiskii, and F. Teppe, *Phys. Rev. Lett.* **120**, 086401 (2018).
- [6] J. Ludwig, Y. B. Vasilyev, N. N. Mikhailov, J. M. Pomirol, Z. Jiang, O. Vafek, and D. Smirnov, *Phys. Rev. B* **89**, 241406(R) (2014).
- [7] M. Marcinkiewicz, S. Ruffenach, S. S. Krishtopenko, A. M. Kadykov, C. Consejo, D. B. But, W. Desrat, W. Knap, J. Torres, A. V. Ikonnikov, K. E. Spirin, S. V. Morozov, V. I. Gavrilenko, N. N. Mikhailov, S. A. Dvoretiskii, and F. Teppe, *Phys. Rev. B* **96**, 035405 (2017).
- [8] S. S. Krishtopenko, I. Yahniuk, D. B. But, V. I. Gavrilenko, W. Knap, and F. Teppe, *Phys. Rev. B* **94**, 245402 (2016).
- [9] S. Wiedmann, A. Jost, C. Thienel, C. Brüne, P. Leubner, H. Buhmann, L. W. Molenkamp, J. C. Maan, and U. Zeitler, *Phys. Rev. B* **91**, 205311 (2015).
- [10] A. V. Ikonnikov, S. S. Krishtopenko, O. Drachenko, M. Goiran, M. S. Zholudev, V. V. Platonov, Y. B. Kudasov, A. S. Korshunov, D. A. Maslov, I. V. Makarov, O. M. Surdin, A. V. Philippov, M. Marcinkiewicz, S. Ruffenach, F. Teppe, W. Knap, N. N. Mikhailov, S. A. Dvoretzky, and V. I. Gavrilenko, *Phys. Rev. B* **94**, 155421 (2016).
- [11] P. Leubner, L. Lunczer, C. Brüne, H. Buhmann, and L. W. Molenkamp, *Phys. Rev. Lett.* **117**, 086403 (2016).
- [12] I. Yahniuk, S. S. Krishtopenko, G. Grabecki, B. Jouault, C. Consejo, W. Desrat, M. Majewicz, A. M. Kadykov, K. E. Spirin, V. I. Gavrilenko, N. N. Mikhailov, S. A. Dvoretzky, D. B. But, F. Teppe, J. Wrobel, G. Cywinski, S. Kret, T. Dietl, and W. Knap, *npj Quantum Mater.* **4**, 13 (2019).
- [13] S. S. Krishtopenko, M. Antezza, and F. Teppe, *Phys. Rev. B* **101**, 205424 (2020).
- [14] C. Liu, T. L. Hughes, X.-L. Qi, K. Wang, and S.-C. Zhang, *Phys. Rev. Lett.* **100**, 236601 (2008).
- [15] M. König, H. Buhmann, L. W. Molenkamp, T. Hughes, C.-X. Liu, X.-L. Qi, and S.-C. Zhang, *J. Phys. Soc. Jpn.* **77**, 031007 (2008).
- [16] M. V. Durnev and S. A. Tarasenko, *Phys. Rev. B* **93**, 075434 (2016).
- [17] C. Brüne, A. Roth, H. Buhmann, E. M. Hankiewicz, L. W. Molenkamp, J. Maciejko, X.-L. Qi, and S.-C. Zhang, *Nat. Phys.* **8**, 485 (2012).
- [18] E. Olshanetsky, Z. Kvon, G. Gusev, N. Mikhailov, and S. Dvoretzky, *Phys. E: Low-Dimensional Syst. Nanostruct.* **99**, 335 (2018).
- [19] A. M. Kadykov, F. Teppe, C. Consejo, L. Viti, M. S. Vitiello, S. S. Krishtopenko, S. Ruffenach, S. V. Morozov, M. Marcinkiewicz, W. Desrat, N. Dyakonova, W. Knap, V. I. Gavrilenko, N. N. Mikhailov, and S. A. Dvoretzky, *Appl. Phys. Lett.* **107**, 152101 (2015).
- [20] A. M. Kadykov, J. Torres, S. S. Krishtopenko, C. Consejo, S. Ruffenach, M. Marcinkiewicz, D. But, W. Knap, S. V. Morozov, V. I. Gavrilenko, N. N. Mikhailov, S. A. Dvoretzky, and F. Teppe, *Appl. Phys. Lett.* **108**, 262102 (2016).
- [21] M. Orlita, K. Masztalerz, C. Faugeras, M. Potemski, E. G. Novik, C. Brüne, H. Buhmann, and L. W. Molenkamp, *Phys. Rev. B* **83**, 115307 (2011).
- [22] M. Zholudev, F. Teppe, M. Orlita, C. Consejo, J. Torres, N. Dyakonova, M. Czapkiewicz, J. Wróbel, G. Grabecki, N. Mikhailov, S. Dvoretzky, A. Ikonnikov, K. Spirin, V. Aleshkin, V. Gavrilenko, and W. Knap, *Phys. Rev. B* **86**, 205420 (2012).

- [23] M. S. Zholudev, F. Teppe, S. V. Morozov, M. Orlita, C. Consejo, S. Ruffenach, W. Knap, V. I. Gavrilenko, S. A. Dvoretiskii, and N. N. Mikhailov, *JETP Lett.* **100**, 790 (2015).
- [24] L. S. Bovkun, A. V. Ikonnikov, V. Y. Aleshkin, K. E. Spirin, V. I. Gavrilenko, N. Mikhailov, S. A. Dvoretzky, F. Teppe, B. A. Piot, M. Potemski, and M. Orlita, *J. Phys.: Condens. Matter* **31**, 145501 (2019).
- [25] S. A. Tarasenko, M. V. Durnev, M. O. Nestoklon, E. L. Ivchenko, J.-W. Luo, and A. Zunger, *Phys. Rev. B* **91**, 081302(R) (2015).
- [26] G. M. Minkov, A. V. Germanenko, O. E. Rut, A. A. Sherstobitov, M. O. Nestoklon, S. A. Dvoretzki, and N. N. Mikhailov, *Phys. Rev. B* **93**, 155304 (2016).
- [27] Y. A. Bychkov, S. V. Iordanskii, and G. M. Eliashberg, *JETP Lett.* **33**, 143 (1981).
- [28] C. Kallin and B. I. Halperin, *Phys. Rev. B* **30**, 5655 (1984).
- [29] A. H. MacDonald and C. Kallin, *Phys. Rev. B* **40**, 5795 (1989).
- [30] Y. A. Bychkov and G. Martinez, *Phys. Rev. B* **66**, 193312 (2002).
- [31] W. Kohn, *Phys. Rev.* **123**, 1242 (1961).
- [32] S. S. Krishtopenko, *J. Phys.: Condens. Matter* **25**, 365602 (2013).
- [33] S. S. Krishtopenko, A. V. Ikonnikov, M. Orlita, Y. G. Sadofyev, M. Goiran, F. Teppe, W. Knap, and V. I. Gavrilenko, *J. Appl. Phys.* **117**, 112813 (2015).
- [34] H. Arimoto, N. Miura, and R. A. Stradling, *Phys. Rev. B* **67**, 155319 (2003).
- [35] C. M. Hu, C. Zehnder, C. Heyn, and D. Heitmann, *Phys. Rev. B* **67**, 201302(R) (2003).
- [36] S. S. Krishtopenko, V. I. Gavrilenko, and M. Goiran, *Solid State Phenom.* **190**, 554 (2012).
- [37] S. S. Krishtopenko and F. Teppe, *Sci. Adv.* **4**, eaap7529 (2018).
- [38] Z. Jiang, E. A. Henriksen, L. C. Tung, Y.-J. Wang, M. E. Schwartz, M. Y. Han, P. Kim, and H. L. Stormer, *Phys. Rev. Lett.* **98**, 197403 (2007).
- [39] E. A. Henriksen, P. Cadden-Zimansky, Z. Jiang, Z. Q. Li, L.-C. Tung, M. E. Schwartz, M. Takita, Y.-J. Wang, P. Kim, and H. L. Stormer, *Phys. Rev. Lett.* **104**, 067404 (2010).
- [40] C. Faugeras, S. Berciaud, P. Leszczynski, Y. Henni, K. Nogajewski, M. Orlita, T. Taniguchi, K. Watanabe, C. Forsythe, P. Kim, R. Jalil, A. K. Geim, D. M. Basko, and M. Potemski, *Phys. Rev. Lett.* **114**, 126804 (2015).
- [41] B. J. Russell, B. Zhou, T. Taniguchi, K. Watanabe, and E. A. Henriksen, *Phys. Rev. Lett.* **120**, 047401 (2018).
- [42] K. E. Spirin, K. P. Kalinin, S. S. Krishtopenko, K. V. Maremyanin, V. I. Gavrilenko, and Y. G. Sadofyev, *Semiconductors* **46**, 1396 (2012).
- [43] S. S. Krishtopenko, W. Desrat, K. E. Spirin, C. Consejo, S. Ruffenach, F. Gonzalez-Posada, B. Jouault, W. Knap, K. V. Maremyanin, V. I. Gavrilenko, G. Boissier, J. Torres, M. Zaknoute, E. Tournié, and F. Teppe, *Phys. Rev. B* **99**, 121405(R) (2019).
- [44] See Supplemental Material at <http://link.aps.org/supplemental/10.1103/PhysRevB.102.041404>, which also contains Refs. [49–51], for a brief discussion of the joint effect of SIA, BIA, and IIA on Landau levels within the Dirac-like BHZ model. Analysis of magnetoabsorption spectra of the sample 101221 and details of the spectra for the samples 101109 and 091223 are also provided therein.
- [45] M. Schultz, U. Merkt, A. Sonntag, U. Rössler, R. Winkler, T. Colin, P. Helgesen, T. Skauli, and S. Løvold, *Phys. Rev. B* **57**, 14772 (1998).
- [46] S. Dvoretzky, N. Mikhailov, Y. Sidorov, V. Shvets, S. Danilov, B. Wittman, and S. Ganichev, *J. Electron. Mater.* **39**, 918 (2010).
- [47] F. Teppe, M. Marcinkiewicz, S. S. Krishtopenko, S. Ruffenach, C. Consejo, A. M. Kadykov, W. Desrat, D. But, W. Knap, J. Ludwig, S. Moon, D. Smirnov, M. Orlita, Z. Jiang, S. V. Morozov, V. Gavrilenko, N. N. Mikhailov, and S. A. Dvoretiskii, *Nat. Commun.* **7**, 12576 (2016).
- [48] K. E. Spirin, D. M. Gaponova, V. I. Gavrilenko, N. N. Mikhailov, and S. A. Dvoretzky, *Semiconductors* **53**, 1363 (2019).
- [49] S. S. Krishtopenko, *Semicond. Sci. Technol.* **29**, 085005 (2014).
- [50] S. S. Krishtopenko, W. Knap, and F. Teppe, *Sci. Rep.* **6**, 30755 (2016).
- [51] A. A. Dobretsova, Z. D. Kvon, S. S. Krishtopenko, N. N. Mikhailov, and S. A. Dvoretzky, *J. Low Temp. Phys.* **45**, 159 (2019).